AD-A059 001 DAYTON UNIV OHIO RESEARCH INST F/G 10/3
A FEASIBILITY STUDY OF INORGANIC OXIDE-FLUORIDE COMPOSITIONS FO--ETC(U)
APR 78 J E DAVISON AFOSR-77-3117
UNCLASSIFIED UDRI-TR-78-41 AFOSR-TR-78-1145 NL

END
DATE FILMED
11-78
DDC

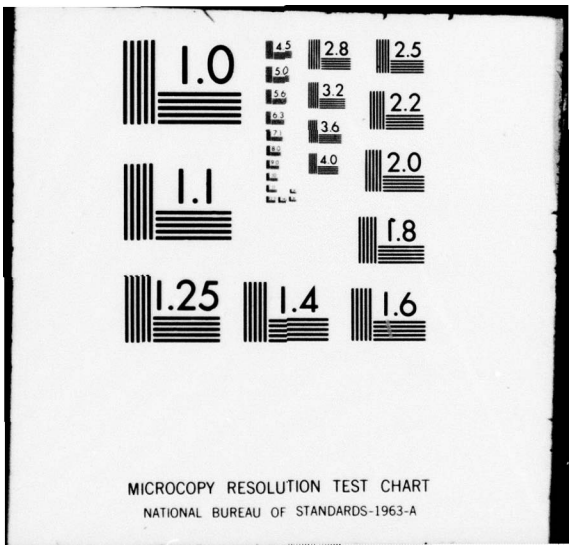
1.0
1.1
1.25
1.4
1.6
1.8
2.0
2.2
2.5
2.8
3.2
3.6
4.0
4.5
5.0
5.6
MICROCOPY RESOLUTION TEST CHART
NATIONAL BUREAU OF STANDARDS-1963-A

AFOSR-TR- 78-1145

UDRI-TR-78-41

LEVEL II



# A FEASIBILITY STUDY OF INORGANIC OXIDE-FLUORIDE COMPOSITIONS FOR THERMAL ENERGY STORAGE APPLICATIONS

J. E. Davison

UNIVERSITY OF DAYTON
RESEARCH INSTITUTE
DAYTON, OHIO 45469



AFOSR Grant 77-3117

APRIL 1978

UNCLASSIFIED

SECURITY CLASSIFICATION OF THIS PAGE *(When Data Entered)*

## REPORT DOCUMENTATION PAGE

READ INSTRUCTIONS BEFORE COMPLETING FORM

1. REPORT NUMBER: AFOSR-TR-78-1145
2. GOVT ACCESSION NO.
3. RECIPIENT'S CATALOG NUMBER
4. TITLE (and Subtitle): A FEASIBILITY STUDY OF INORGANIC OXIDE-FLUORIDE COMPOSITIONS FOR THERMAL ENERGY STORAGE APPLICATIONS
5. TYPE OF REPORT & PERIOD COVERED: Final Rept.
6. PERFORMING ORG. REPORT NUMBER
7. AUTHOR(s): J. E. Davison
8. CONTRACT OR GRANT NUMBER(s): AFOSR-77-3117
9. PERFORMING ORGANIZATION NAME AND ADDRESS: University of Dayton Research Institute, Dayton, OH 45469
10. PROGRAM ELEMENT, PROJECT, TASK AREA & WORK UNIT NUMBERS: 2301/A5, 61102F; A5
11. CONTROLLING OFFICE NAME AND ADDRESS: AFOSR/NP, Bolling AFB, Bldg.#410, Wash DC 20332
12. REPORT DATE: April 1978
13. NUMBER OF PAGES: 52
14. MONITORING AGENCY NAME & ADDRESS *(if different from Controlling Office)*
15. SECURITY CLASS. *(of this report)*: Unclassified
15a. DECLASSIFICATION/DOWNGRADING SCHEDULE
16. DISTRIBUTION STATEMENT *(of this Report)*: Approved for public release; distribution unlimited. 56 p.
17. DISTRIBUTION STATEMENT *(of the abstract entered in Block 20, if different from Report)*: UDRI-TR-78-41
18. SUPPLEMENTARY NOTES
19. KEY WORDS *(Continue on reverse side if necessary and identify by block number)*
20. ABSTRACT *(Continue on reverse side if necessary and identify by block number)*

The purpose of this present investigation was to review the liquid-solid transformations of chemical compositions intermediate between pure inorganic fluorides and pure inorganic oxides. The liquid-solid transformations of seventy oxide-fluoride systems were reviewed. Five of these oxide-fluoride systems were identified which have liquid-solid transformations in the desired temperature interval. The values of the enthalpy of the liquid-solid transformation, the eutectic temperature, the thermal diffusivity, and the density of the liquid and solid phases were measured. These measured values were compared to the values

DD FORM 1 JAN 73 1473 EDITION OF 1 NOV 65 IS OBSOLETE

105 400

UNCLASSIFIED

SECURITY CLASSIFICATION OF THIS PAGE *(When Data Entered)*

which had been measured on inorganic eutectic fluorides. As a result of this comparison, the LiF-MgF2-KF eutectic composition is recommended for thermal energy storage application because of the larger value for the enthalpy of transformation.

TABLE OF CONTENTS



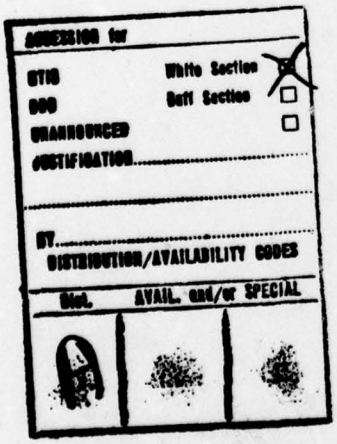

## 1.0 INTRODUCTION AND SUMMARY

The University of Dayton has conducted an investigation of chemical compositions of inorganic oxide-fluoride systems to determine their potential for thermal energy storage applications in space vehicles. In previous investigations on Air Force Contracts, F33615-76-C-2096, F33601-75-32821, and F33601-75-32822, the feasibility of utilizing the liquid-solid transformations of inorganic oxides were investigated. The values for the enthalpy of fusion of selected inorganic oxides are two to three times those of the best inorganic fluoride, lithium fluoride. A potential application for these thermal energy storage materials is the operation of a Vuilleumier Spacecraft Cryocooler. The temperature interval of interest for thermal storage in this application is 1000-1400°F (537-760°C). The inorganic oxides which possess large values for their enthalpy of fusion melt at temperatures well above this temperature interval. The purpose of this present investigation was to review the liquid-solid transformations of chemical compositions intermediate between pure inorganic fluorides and pure inorganic oxides. The liquid-solid transformations of seventy oxide-fluoride systems were reviewed. Five of these oxide-fluoride systems were identified which have liquid-solid transformations in the desired temperature interval. Based on an estimate of the enthalpy of transformation and the temperature of the eutectic transformation, the eutectic composition at 20 weight percent lithium fluoride of the $LiF-Li_2O-B_2O_3$ system was selected for experimental characterization. The values of the enthalpy of the liquid-solid transformation, the eutectic temperature, the thermal diffusivity, and the density of the liquid and solid phases were measured. These measured values were compared to the values which had been measured on inorganic eutectic fluorides. As a result of this comparison, the $LiF-MgF_2-KF$ eutectic composition is recommended for thermal energy storage application because of the larger value for the enthalpy of transformation. However, the lack of phase diagrams or other data on the liquid-solid transformations within oxide-fluoride systems has precluded an exhaustive assessment of the potential of these systems. There are no oxide-fluoride

phase diagrams available in which one of the oxides, $ThO_2$, BeO, VO, or T:O, is a component. All of these oxides have values for their enthalpy of fusion which is greater than 850 Joules per gram and the oxide, $ThO_2$, has a value for the enthalpy of fusion which is 4610 Joules per gram.

## 2.0 ANALYTICAL STUDIES

The assessment of the liquid-solid transformations was performed to select an optimal composition for further experimental characterization. In previous investigations* inorganic fluorides and inorganic oxides had been separately evaluated to determine their performance as the energy storage media for thermal energy storage applications although inorganic oxides were identified with enthalpies of fusion which are much larger than any of the inorganic fluorides, the melting points of the oxides are correspondingly higher than the fluorides. The high melting temperatures of these oxides makes them unsuitable for applications in the temperature interval of 1000-1400°F (539-760°C). In the present study, the liquid-solid transformations of chemical compositions which are intermediate between a pure oxide and a pure fluoride were assessed to determine their potential for thermal storage applications.

The pure inorganic oxides and fluorides which were considered in this study were selected on the basis of the value for the enthalpy of fusion per unit weight of the pure component. Those substances which have a value for the enthalpy of fusion which is greater than 100 watt hours per pound (0.794 kilo Joules per gram) were selected for further study. Nine pure oxides and three pure fluorides have values which exceed this value. These substances, their values for the enthalpy of fusion, and their melting temperatures are presented in Table 1.

* AFAPL-TR-77-70,"Feasibility Study of Inorganic Oxides for TES Applications" and, AFAPL-TR-75-92,"Evaluation of Eutectic TES Unit Compatibility," Air Force Aero-Propulsion Laboratory, Wright-Patterson Air Force Base, Ohio 45433.

TABLE 1

ENTHALPY OF FUSION AND MELTING TEMPERATURE
OF SELECTED INORGANIC OXIDES AND FLUORIDES

| | Enthalpy of Fusion KJ/g | watt-hr/lb | Melting Temperature Deg. K | Deg. F | Ref. |
|---|---|---|---|---|---|
| OXIDES | | | | | |
| $ThO_2$ | 4.61 | 581 | 3225 | 5346 | 2 |
| BeO | 2.53 | 318 | 2820 | 4617 | 1 |
| $Li_2O$ | 1.96 | 247 | 1843 | 2858 | 1 |
| MgO | 1.92 | 242 | 3098 | 5117 | 1 |
| $Al_2O_3$ | 1.161 | 146 | 2315 | 3708 | 1 |
| VO | 0.938 | 118 | 2350 | 3771 | 2 |
| CaO | 0.895 | 113 | 2873 | 4712 | 2 |
| TiO | 0.851 | 107 | 2023 | 3182 | 1 |
| $TiO_2$ | 0.838 | 106 | 2143 | 3398 | 1 |
| FLUORIDES | | | | | |
| LiF | 1.044 | 132 | 1121 | 1560 | 1 |
| $MgF_2$ | 0.933 | 118 | 1536 | 2305 | 1 |
| NaF | 0.794 | 100 | 1269 | 1825 | 1 |

1 JANAF Thermochemical Tables, 2nd Edition, Dow Chemical Dow Chemical Company, Midland, Michigan.

2 Wicks and Block, Thermodynamic Properties of 65 Elements, Bureau of Mines Bulletin 605, 1963.

## 2.1 Inorganic Oxide-Fluoride Systems

The temperature of the liquid-solid transformations of compositions which are intermediate between a pure oxide and a pure fluoride were determined from their temperature-composition phase diagrams. The review of the phase diagrams of oxide-fluoride systems was limited to those systems which contain at least one of the substances listed in Table 1. The binary and ternary phase diagrams which were reviewed are presented in Table 2. (It was noted that phase diagrams of oxide-fluoride systems which contain either $ThO_2$, BeO, VO, or TiO, have apparently attracted little research interest since none were found in the compilations of Phase Diagrams for Ceramists.) The temperatures of the liquid-solid transformations were used as a criterion for selecting systems of potential interest. The review of these transformations for all of the oxide-fluoride systems which were considered is presented in Appendix A. Five of the oxide-fluoride systems have transformation temperatures in the interval of 537 to 760°C. These systems are reviewed in the following paragraphs.

$LiF-B_2O_3-Li_2O$

The compound, $LiBO_2$, melts at a temperature of 843°C. The compound $2LiF \cdot 3LiBO_2$ melts at a temperature of 755°C. The eutectic reaction between $LiBO_2$ and $2LiF \cdot 3LiBO_2$ occurs at 710°C and at 20 percent LiF. The eutectic reaction between LiF and $2LiF \cdot 3LiBO_2$ occurs at 688°C and at 35 percent LiF.

$LiF-Li_2O-MoO_3$

The compound, $Li_2MoO_4$, melts without a change in composition at 700°C. An eutectic exists at 62 mole percent $Li_2MoO_4$ at a temperature of 620°C between the solid phases, LiF and $Li_2MoO_4$.

$LiF-Li_2O-V_2O_5$

The compound, $LiVO_3$, melts at 621°C. An eutectic between $LiVO_3$ and LiF exists at a temperature of 583°C and at a composition of 75 mole percent $LiVO_3$.

TABLE 2

BINARY AND TERNARY INORGANIC OXIDE-FLUORIDE SYSTEMS WHICH WERE REVIEWED FOR POTENTIAL IN THERMAL ENERGY STORAGE SYSTEMS

---

$LiF-B_2O_3$
$-AlF_3-Al_2O_3$
$-B_2O_3-BaF_2$
$-B_2O_3-Li_2O$
$-GeO-MgO$
$-K_2O-TiO_2$
$-Li_2O-MoO_3$
$-Li_2O-V_2O_5$
$-Li_2O-WO_3$

$Li_2O-B_2O_3-LiF$
$-KF-TiO_2$
$-LiF-MoO_3$
$-LiF-V_2O_5$
$-LiF-WO_3$
$-NaF-TiO_2$
$-RbF-TiO_2$

$CaO-CaF_2$
$-AlF_3-NaF$
$-Al_2O_3-CaF_2$
$-CaF_2-FeO$
$-CaF_2-MgO$
$-CaF_2-P_2O_5$
$-CaF_2-SiO_2$

$MgF_2-MgO$
$-GeO-MgO$
$-KF-SiO_2$
$-MgO-SiO_2$
$-NaF-SiO_2$

$NaF-CrO_3-Na_2O$
$-Li_2O-TiO_2$
$-Na_2O-MoO_3$
$-Na_2O-P_2O_5$
$-Na_2O-SiO_2$
$-Na_2O-TiO_2$
$-Na_2O-V_2O_5$
$-Na_2O-WO_3$
$-PbO-TiO_2$
$-SiO_2-SrF_2$

$Al_2O_3-CaF$
$-NaF$
$-AlF_3-LiF$
$-AlF_3-NaF$
$-CaF_2-CaO$
$-CaF_2-SiO_2$
$-CaF_2-TiO_2$

$NaF-Al_2O_3$
$-AlF_3-Al_2O_3$
$-AlF_3-CaO$
$-AlF_3-CdO$
$-AlF_3-CeO_2$
$-AlF_3-MgO$
$-AlF_3-Nd_2O_3$
$-AlF_3-Sm_2O_3$
$-AlF_3-TiO_2$
$-AlF_3-ZnO$
$-AlF_3-ZrO$
$-B_2O_3-Na_2O$
$-BaF_2-SiO_2$
$-BaO-TiO_2$
$-CaF_2-SiO_2$

$MgO-CaF_2$
$-MgF_2$
$-AlF_3-NaF$
$-CaF_2-CaO$
$-CaF_2-SiO_2$
$-GeO_2-LiF$
$-GeO_2-MgF_2$
$-MgF_2-SiO_2$

TABLE 2 (concluded)

BINARY AND TERNARY INORGANIC OXIDE-FLUORIDE SYSTEMS WHICH WERE REVIEWED FOR POTENTIAL IN THERMAL ENERGY STORAGE SYSTEMS

---

$TiO_2$-CaF
-$AlF_3$-NaF
-$Al_2O_3$-$CaF_2$
-BaO-KF
-BaO-NaF
-KF-$Li_2O$
-Kf-PbO
-$K_2O$-LiF
-$Li_2O$-NaF
-$Li_2O$-RbF
-NaF-$Na_2O$
-NaF-PbO

$LiF-Li_2O-WO_3$

The compound, $Li_2WO_4$, melts congruently at a temperature of 740°C. The eutectic between $Li_2WO_4$ and LiF is at 640°C and at a composition of 62 mole percent $Li_2WO_4$.

$NaF-B_2O_3-Na_2O$

The compound, $Na_2B_4O_7$, melts congruently at a temperature of 742°C. An eutectic reaction between this compound and sodium fluoride occurs at a temperature of 680°C and at a composition of 20 mole percent $Na_2F_2$.

2.1.1 Enthalpy of Transformation

The values for the enthalpy of transformation were estimated for the oxide-fluoride compositions selected in Section 2.1. The enthalpy of transformation of the intermediate composition was calculated from the expression,

$$\Delta H = n_A \Delta H_{f\,A} + n_B \Delta H_{fB}, \qquad (1)$$

where symbols, $\Delta H_{fA}$ and $\Delta H_{fB}$, are the enthalpies of fusion of the pure components and $n_A$ and $n_B$ represent the chemical proportions of the two pure components. This estimate neglects the contribution of the difference between the heat capacities of the liquid and solid phases and the contribution of the enthalpies of the chemical reactions between the pure components. The thermodynamic basis for this method is fully developed and presented in Appendix B. The values which were calculated are presented in Table 3. Experimental values, where they were available, are included in this compilation. In addition to the five oxide-fluoride systems which were identified in Section 2.1, values were estimated for four other systems. Among all of the systems presented in Table 3, the system, $NaF-Li_2O-TiO_2$, has a composition with the largest value for the enthalpy of transformation. Unfortunately, the eutectic temperature is more than 100°C higher than the temperature interval of current interest. Based on the estimated values of the enthalpy of transformation, the eutectic composition of the $LiF-B_2O_3-Li_2O$ system located at twenty weight percent LiF and 710°C was selected for experimental characterization.

TABLE 3

ESTIMATED AND EXPERIMENTAL VALUES OF THE ENTHALPY OF LIQUID-SOLID TRANSFORMATIONS OF SELECTED INORGANIC OXIDE-FLUORIDE COMPOSITIONS

| System | Composition | Type | Transformation Temperature Deg C | Enthalpy KJ/g |
|---|---|---|---|---|
| $LiF-B_2O_3$ | 1. $LiF \cdot B_2O_3$ | C | 840 | 0.513 |
| | 2. $N_{LiF}=0.5$ | E | 798 | 0.627 |
| $LiF-AlF_3-Al_2O_3$ | $N_{Al_2O_3}=0.01$ | E | 775 | 0.533 |
| $LiF-B_2O_3-Li_2O$ | 1. $LiBO_2$ | C | 844 | 0.681* |
| | 2. $2LiF \cdot 3LiBO_2$ | C | 755 | 0.774 |
| | 3. wt.% LiF=0.2 | E | 710 | 0.755 |
| $LiF-Li_2O-MoO_3$ | 1. $Li_2MoO_4$ | C | 700 | 0.276 |
| | 2. $N_{LiF}=0.4$ | E | 620 | 0.344 |
| $LiF-Li_2O-V_2O_5$ | 1. $LiVO_3$ | C | 621 | 0.585 |
| | 2. $N_{LiF}=0.25$ | E | 583 | 0.619 |
| $LiF-Li_2O-WO_3$ | 1. $Li_2WO_4$ | C | 740 | 0.449 |
| | 2. $N_{LiF}=0.4$ | E | 640 | 0.230 |
| $NaF-Al_2O_3-CaO$ | 1. $Na_3AlF_6$ | C | 1012 | 0.511* |
| | 2. $N_{CaO}=0.11$ | E | 896 | 0.598 |
| $NaF-B_2O_3-Na_2O$ | 1. $Na_2B_4O_7$ | C | 742 | 0.403* |
| | 2. $N_{NaF}=0.2$ | E | 680 | 0.495 |
| $NaF-Li_2O-TiO_2$ | 1. $Li_2TiO_3$ | C | 1547 | 1.004* |
| | 2. $N_{NaF}=0.75$ | E | 874 | 0.984 |

*Experimental values, see JANAF Thermochemical Tables 2nd Edition, Dow Chemical Company, Midland, Michigan, July 1970.

## 2.2 Alloy Container Compatibility

The chemical compatibility between the oxide-fluoride composition and metal alloy containers was assessed by considering the possibility for simple oxidation-reduction reactions to occur between the two materials. The values for the Gibbs free energy of formation of the stable compounds was used as the quantitative basis for this assessment. The values for the free energy of formation of the pure components of the oxide-fluoride composition were compared to those of the pure elemental constituents of stainless steels and nickel-based alloys. This comparison provides a quantitative measure for determining if chemical reactions of the type

$$\frac{1}{2}\,Ni + LiF \rightarrow \frac{1}{2}\,NiF + Li, \text{ or}$$

$$Ni + Li_2O \rightarrow NiO + 2Li,$$

are thermodynamically favored to occur. The elemental constituents of stainless steel and nickel-based allows are listed in Table 4. The values for the free energy of formation of the stable oxides and fluorides of these elements and the compounds of the selected oxide-fluoride composition are listed in Tables 5a and 5b. The comparison of these values indicates that lithium fluoride is more stable than the fluorides of any of the elemental constituents of the metal containers. Thus, no oxidation-reduction reactions are expected to occur involving the lithium fluoride and either stainless steel or nickel-based alloys. The comparison of the values among the oxides shows that the boron oxide can be reduced by the pure elements magnesium, lithium, aluminum, titanium, and silicon. The comparison for the dilithium oxide shows that only magnesium is thermodynamically favored to reduce this oxide at all of the indicated temperatures. At a temperature of 1500K, the element aluminum is also favored to reduce the dilithium oxide. Since the composition of many of the stainless steels and nickel alloys contain magnesium, silicon, titanium, or aluminum as minor alloying constituents, the performance of an alloy containing any of these elements should be experimentally characterized before its final selection.

TABLE 4

ELEMENTAL ALLOYING CONSTITUENTS OF
STAINLESS STEEL AND NICKEL-BASED ALLOYS

| | |
|---|---|
| iron | selenium |
| nickel | molybdenum |
| chromium | titanium |
| aluminum | sulfur |
| carbon | copper |
| magnesium | columbium |
| manganese | tantalum |
| silicon | phosphorus |
| cobalt | |

TABLE 5a

GIBBS FREE ENERGY OF FORMATION OF SELECTED FLUORIDES
(Values from JANAF Thermochemical Tables)
$-\Delta G$ per Fluoride atom in Kilo Calories

| | (Deg K) | | | |
|---|---|---|---|---|
| Fluoride | 298 | 500 | 1000 | 1500 |
| LiF | 140.70 | 136.08 | 124.34 | 113.31 |
| $MgF_2$ | 128.00 | 123.76 | 113.53 | 101.80 |
| $AlF_3$ | 114.02 | 109.78 | 99.59 | 89.31 |
| $TiF_3$ | 108.50 | 104.62 | 95.42 | 86.58 |
| $SiF_4$ | 93.96 | 92.23 | 87.89 | 83.56 |
| $TiF_4$ | 93.17 | 89.63 | 81.59 | 74.19 |
| $MnF_2$ | 90.00 | 86.50 | 78.50 | 73.25 |
| $TaF_5$ | ~90.00 | --- | --- | --- |
| $CrF_2$ | 86.00 | 82.75 | 74.00 | 68.50 |
| $CbF_5$ | ~81.00 | --- | --- | --- |
| $FeF_2$ | 79.25 | 75.88 | 67.90 | 59.94 |
| $FeF_3$ | 77.46 | 73.82 | 65.15 | 56.52 |
| $CoF_2$ | 74.88 | 71.35 | 6.315 | 55.25 |
| $MnF_3$ | 74.07 | 70.17 | 63.67 | --- |
| $PF_3$ | 73.69 | 72.78 | 70.94 | 65.50 |
| $NiF_2$ | 73.35 | 70.00 | 62.00 | 54.25 |
| $PF_5$ | 72.12 | 69.88 | 64.65 | 57.35 |
| $CuF_2$ | 59.64 | 55.71 | 46.57 | 37.92 |
| $MoF_6$ | 58.70 | 55.80 | 49.68 | 45.48 |
| $CF_4$ | 53.09 | 51.26 | 46.69 | 42.15 |
| $SF_4$ | 44.21 | 42.49 | 37.57 | 31.33 |
| CuF | 41.04 | 37.81 | 30.88 | 24.62 |
| $SeF_6$ | ~40.00 | --- | --- | --- |

TABLE 5b

GIBBS FREE ENERGY OF FORMATION OF SELECTED OXIDES
(Values from Bureau of Mines Bulletin 542)
$-\Delta G^\circ$ per Oxygen atom of Kilo Calories

| Oxide | Temp. (Deg K) 298 | 500 | 1000 | 1500 |
|---|---|---|---|---|
| MgO | 136.1 | 131.4 | 117.7 | 101.3 |
| $Li_2O$ | 133.8 | 127.5 | 110.2 | 92.1 |
| $Al_2O_3$ | 125.8 | 120.7 | 108.2 | 95.1 |
| TiO | 116.9 | 112.3 | 101.1 | 90.3 |
| $Ti_2O_3$ | 114.1 | 109.5 | 98.9 | 88.7 |
| $Ti_3O_5$ | 110.6 | 106.2 | 96.1 | 86.1 |
| $TiO_2$ | 106.1 | 101.7 | 91.1 | 80.6 |
| $SiO_2$ | 98.4 | 94.1 | 83.4 | 73.1 |
| $B_2O_3$ | 95.5 | 91.2 | 81.7 | 73.3 |
| $Ta_2O_5$ | 91.3 | 87.0 | 76.7 | 66.9 |
| $Cb_2O_4$ | 88.6 | 84.3 | 73.7 | 63.5 |
| MnO | 86.7 | 83.2 | 74.6 | 65.5 |
| $Cb_2O_5$ | 84.6 | 80.3 | 69.9 | 59.9 |
| $Cr_2O_3$ | 84.4 | 80.1 | 69.7 | 59.9 |
| $Mn_3O_4$ | 76.5 | 72.2 | 61.8 | 51.3 |
| $Mn_2O_3$ | 70.2 | 66.1 | 55.9 | 45.7 |
| $P_4O_{10}$ | 65.4 | 60.9 | 50.2 | --- |
| $CrO_2$ | 65.0 | 60.8 | 50.3 | --- |
| $Fe_3O_4$ | 60.8 | 56.7 | 47.5 | 38.5 |
| $MoO_4$ | 60.7 | 58.3 | 48.5 | 38.7 |
| $Fe_2O_3$ | 59.1 | 54.9 | 44.8 | 35.1 |
| FeO | 58.7 | 55.5 | 47.9 | 40.15 |
| $MoO_3$ | 54.0 | 49.9 | 40.2 | --- |
| CoO | 51.6 | 48.0 | 38.8 | 30.5 |
| NiO | 50.6 | 46.1 | 35.1 | 24.3 |
| $CO_2$ | 47.1 | 47.2 | 47.3 | 47.3 |
| $CoO_4$ | 45.5 | 41.3 | 30.9 | --- |
| $CrO_3$ | 40.3 | 36.3 | --- | --- |
| $SO_2$ | 35.9 | 36.0 | --- | --- |
| $Cu_2O$ | 35.0 | 31.5 | 23.3 | 15.7 |
| CO | 32.8 | 37.2 | 47.9 | 58.3 |
| CuO | 31.0 | 26.5 | 16.2 | 6.3 |
| $SeO_2$ | 20.8 | 16.3 | 11.8 | 5.5 |
| Pu | 15.0 | 18.5 | 24.5 | --- |
| SeO | -3.0 | +0.7 | 9.0 | 10.3 |

## 3.0 THERMOPHYSICAL PROPERTY MEASUREMENTS

Selected thermophysical properties of the eutectic composition in the $LiBO_2$-LiF system were experimentally determined. The thermophysical properties which were measured were the enthalpy of the liquid-solid transformation, the temperature of the liquid-solid transformation, the thermal diffusivity of the solid phase as a function of temperature, and the densities of the liquid and solid phases.

### 3.1 The Enthalpy of the Liquid-Solid Transformation

The enthalpy of the liquid-solid transformation was determined from the difference between the values of the heat content of the liquid and solid phases at the eutectic temperature. The values for the heat content were measured with the drop calorimetry method.* In this method, the specimen is brought into thermal equilibrium at the desired temperature and then dropped into a calorimeter where the heat energy transferred from the specimen is measured as it comes into thermal equilibrium at the temperature of the calorimeter.

#### 3.1.1 The Calorimetric Experiment

The experimental arrangement used for the determination of the values of the heat content as a function of temperature is presented in Figure 1. The specimen, 2, is brought into thermal equilibrium in the furnace, 1. The temperature of the specimen is measured with the chromel-alumel thermocouple, 3. After attaining thermal equilibrium in the furnace the specimen is physically dropped into the copper block, 6. The heat energy transferred from the specimen to the copper block causes a temperature rise of the block. The temperature rise is detected by a twelve junction thermopile, 10, and displayed

---

* Kubaschewski, O. and Evans, E., Metallurgical Thermochemistry, Third Edition, pp. 100-105, Pergamon Press, New York, New York, 1958.

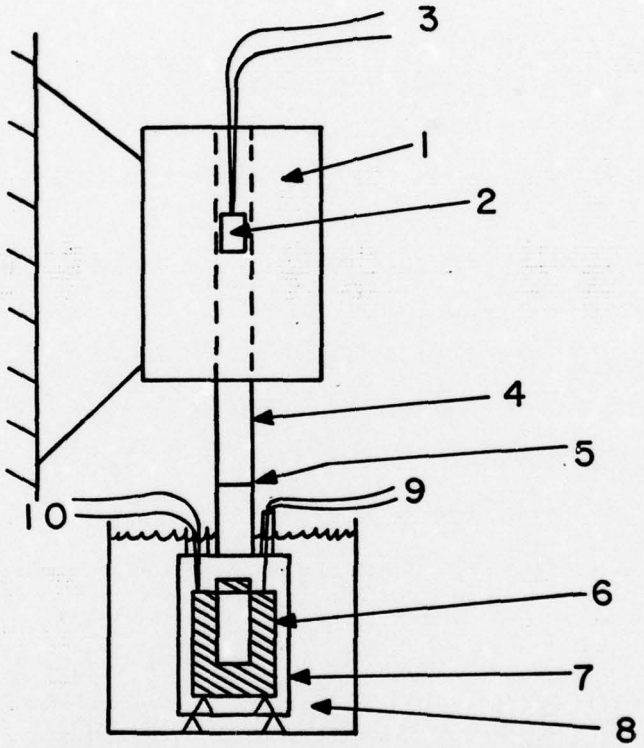


Figure 1. Experimental Arrangement for Measuring the Enthalpy of the Liquid-Solid Transformation.

on a Honeywell Electronik 194 recorder. The copper block is mounted within a water tight container, and the entire subassembly is immersed in an isothermal bath, 8. The cavity of the copper block is fitted with a cover which is closed immediately after the specimen is dropped into the cavity in order to minimize heat losses as the specimen cools. The furnace and the calorimeter subassemblies are connected with an Inconel alloy tube, 4, which contains a gate, 5, which is only opened when the specimen is dropped. The purpose of the gate is to isolate the copper block from the thermal radiation from the furnace cavity. An argon atmosphere is maintained within the calorimeter and furnace subassemblies to prevent oxidation of the specimen during the experiment.

The heat content of the specimen is determined as a function of temperature with respect to the reference temperature from the relation,

$$H(T) - H(T_{ref}) = K\Delta T, \qquad (2)$$

where H(T) denotes the heat content of the specimen at the temperature, T. The reference temperature of the experiments is maintained at 25°C. The symbol, K, represents the calibration constant of the copper block, and the symbol, $\Delta T$, is the temperature rise of the copper block. The product, $K\Delta T$, represents the heat transferred by the specimen as it comes into thermal equilibrium in the copper block.

### 3.1.2 Experimental Results

The measurements of the heat content were conducted on an $LiF\text{-}LiBO_2$ specimen which was prepared at the eutectic composition of 20 weight percent LiF. The measurements were conducted above and below the eutectic temperature. In order to contain the eutectic liquid, the samples were sealed in a type 303 stainless steel capsule. The heat content of the stainless steel had been measured as a function of temperature

in a previous investigation.* The heat content of the eutectic sample was obtained as the difference between the total heat content measured and the heat content of the stainless steel capsule. The calibration constant had been determined by dropping a copper specimen of known mass and correlating the temperature rise of the calorimeter block with the tabulated values of the heat content of copper.** The temperature of the calorimeter block was measured for at least twenty minutes before and after each experimental measurement. The slight changes which were observed in the temperature of the calorimeter block during these time intervals were used to correct the temperature rise which was due to the heat transfer of the specimen. The temperature of the measurements and the values of the heat content of the eutectic specimen are presented in Table 6. The values of the heat content which were determined below the eutectic temperature were fitted as a function of temperature by the method of leasts squares to a linear equation. A similar procedure was performed for the heat content values above the eutectic temperature. The heat content as a function of temperature is given by the equations,

solid, $H(T) - H(25°C) = -203.4 + 2.0818\ T$ joules per gram $T \leq 700$ (3)

liquid, $H(T) - H(25°C) = -198.1 + 3.02252\ T$ joules per gram $725 \leq T$ (4)

The value which is obtained for the enthalpy of the liquid-solid transformation from these expressions is 672 joules per gram.

### 3.2 The Liquid-Solid Transformation Temperature

The liquid-solid transformation of a $LiF\text{-}LiBO_2$ eutectic specimen was measured in a Differential Thermal Analyzer. The

---

* AFAPL-TR-77-70, "Feasibility Study of Inorganic Oxides for Thermal Energy Storage Applications," Air Force Aero Propulsion Laboratory, Wright-Patterson Air Force Base, Ohio 45433.

** Hultgren, et al., Selected Values of Thermophysical Properties of Metals and Alloys, American Society for Metals, Metals Park, Ohio, 1973.

TABLE 6

ENTHALPY OF THE EUTECTIC COMPOSITION,
20 WEIGHT PER LiF at 709°C,
OF THE LiF-$Li_2O$-$B_2O$ SYSTEM

| Temperature Deg C | Enthalpy joules per gram |
|---|---|
| 200 | 213. |
| 300 | 421. |
| 400 | 629. |
| 500 | 838. |
| 600 | 1046. |
| 700 | 1254. |
| 725 | 1993. |
| 750 | 2068. |
| 775 | 2144. |
| 800 | 2220. |

specimen was contained in a type 304 stainless steel capsule. Two complete heating and cooling cycles were performed over the temperature range of 100°C to 790°C. Only one thermal event was observed on the heating and cooling cycles. The temperature of the thermal event on the two heating cycles was observed at 709°C ± 5°C and at 701°C ± 5°C on the two cooling cycles. The slightly lower temperatures observed on the cooling cycles indicate a tendency of the liquid phase to supercool. Thus, the temperature of the transformation observed on the heating cycles is considered to be more representative of the eutectic transformation temperature. The constitution-temperature phase diagram* shows the eutectic transformation temperature for this composition to be at 710°C.

### 3.3 Thermal Diffusivity Measurement

The value of the thermal diffusivity was measured as a function of temperature using the flash technique.** This experimental technique consists of generating a pulse of radiant energy, absorbing the energy pulse on one surface of a flat specimen, and measuring the temperature rise of the opposite surface of the specimen as a function of time. The one-dimensional heat flow equation which describes this experiment has been formulated by Carslaw and Jaeger.*** Under the conditions that the heat pulse is uniformly absorbed in a depth, g, on the surface of an opaque insulated solid of uniform thickness, and where the time duration of the heat pulse is small compared

---

*Levin, E., Robbins, C. and McMurdie, H., Phase Diagrams for Ceramists 1969 Supplement, The American Ceramic Soc., Columbus, Ohio, 1969.

**Parker, W.J., et al., "Flash Method of Determining Thermal Diffusivity, Heat Capacity, and Thermal Conductivity," J. Appl. Phys., 32(9), 1679-1687 (1961).

***Carslaw, W.S. and Jaeger, J.C., Conduction of Heat in Solids, 2nd Edition, Oxford Press, New York, New York, 1959.

to the transit time, then the ratio of the temperature rise of the back surface of the specimen to the maximum temperature rise is given by,

$$\frac{T(\ell,t)}{T_{max}} = 1 + 2 \sum_{n=1} (-1)^n \exp\left(\frac{-n^2\pi^2\alpha t}{\ell^2}\right), \tag{5}$$

where the symbols, $\ell$, $\alpha$, and t, are, respectively, the thickness of the specimen, the thermal diffusivity, and the time. The solution of this expression for the condition,

$$\frac{T(\ell,t)}{T_{max}} = \frac{1}{2}, \tag{6}$$

yields a simple relation among the thermal diffusivity, the specimen thickness, and the time required for the back surface temperature to rise to one-half of its maximum value. This relation is given by,

$$\alpha = \frac{0.139\ell^2}{\tau_{1/2}}. \tag{7}$$

The radiant energy was generated by a power supply which triggered a Xenon flash tube. The pulse is impinged on the surface of the specimen and simultaneously triggers the circuit to mark the time base for the experiment. The specimen was mounted in a spring loaded fixture which was thermally insulated to minimize heat losses. The back surface temperature response of the specimen was sensed by a chromel-alumel thermocouple. The emf output of this thermocouple is amplified and displayed on a monitor oscilloscope and recorded on a waveform recorder. The waveform recorder provides digital storage of the high speed transient electrical signal generated by the back surface thermocouple for subsequent playback at a time compatible with the writing speed of a conventional x-time recorder.

The measurements at elevated temperature were obtained by heating the specimen in a wire-wound resistance furnace. The temperature of the specimen was measured by a separate thermocouple. The front surface of the specimen was coated with a dry

graphitic film lubricant to prevent radiative coupling of the radiant energy with the back surface thermocouple.

### 3.3.1 Experimental Results

Experimental measurements of the thermal diffusivity were conducted for temperatures in the range of 17°C to 501°C. A typical experimental plot of the back surface temperature rise of the specimen as a function of time is presented in Figure 2. The values of the thermal diffusivity were calculated with the aid of Equation 7 from the measured values of the time required for the back surface temperature to rise to one-half of its maximum value and the thickness of the specimen. The experimental data are presented in Table 7. The values of the thermal diffusivity were fitted to a third order polynomial by the method of least squares. The expression for the thermal diffusivity as a function of temperature is given by,

$$\alpha = 0.0175 - 0.4355 \times 10^{-4}T + 0.7710 \times 10^{-7}T^2 - 0.5204 \times 10^{-10}T^3 \quad (8)$$

## 3.4 Liquid Density Measurements

The value for the density of the liquid phase of the eutectic composition of the $LiBO_2$-LiF at twenty weight percent LiF was measured by an adaptation of the maximum bubble pressure method.* In this experiment a stainless steel capillary tube was immersed in the liquid phase and an inert gas was bubbled through the liquid. The pressure of the inert gas, P, within the bubble as it forms on the end of the capillary is related to the surface tension of the liquid, $\delta$, the radius of the bubble, r, the immersion depth of the capillary tube below the surface of the liquid, h, and the densities of the liquid and

*Kingery, W.D., Property Measurements at High Temperatures, John Wiley and Sons, Inc., New York, New York, 1959.

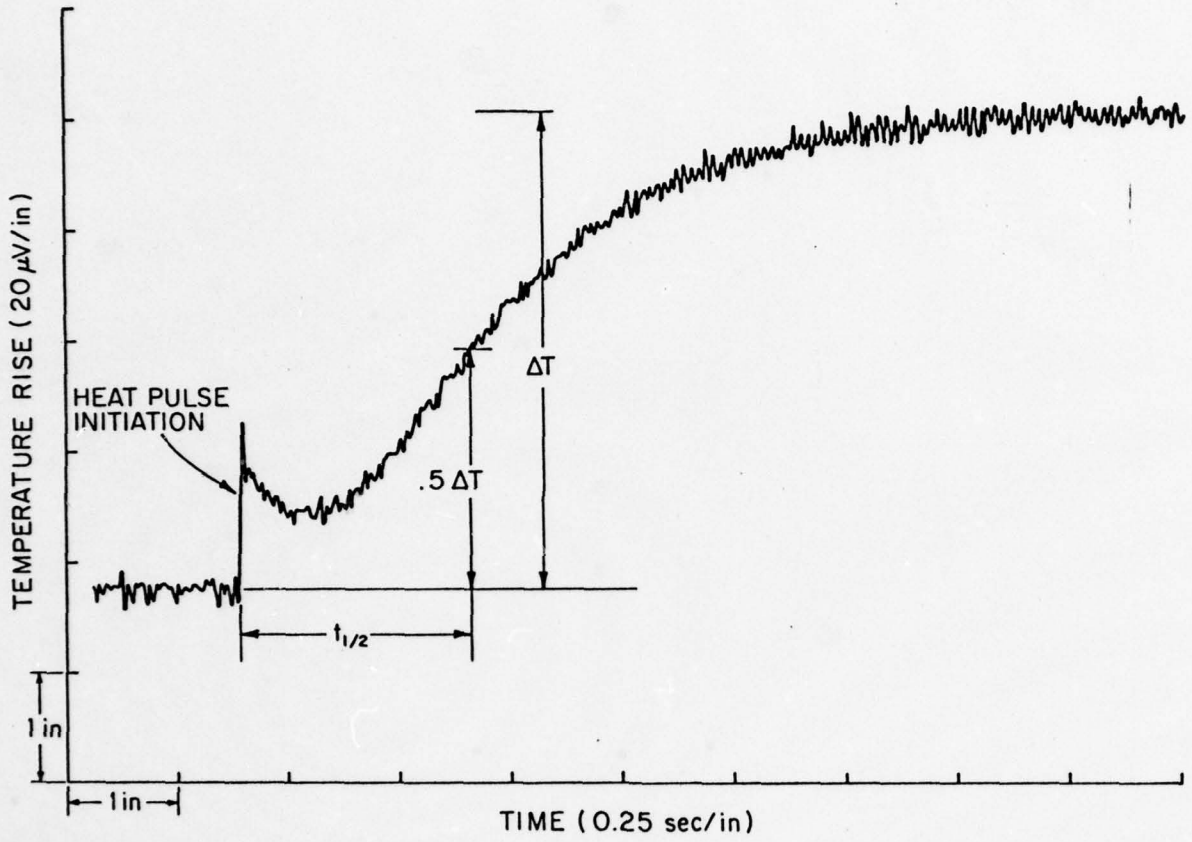


Figure 2. Typical Plot of Temperature of the Back Surface as a Function of Time for Thermal Diffusivity Determinations.

TABLE 7

VALUES FOR THE THERMAL DIFFUSIVITY OF THE $LiF-Li_2O-B_2O_3$ EUTECTIC COMPOSITION

| Temperature Deg C | Thermal Diffusivity $cm^2/sec$ | Temperature Deg C | Thermal Diffusivity $cm^2/sec$ |
|---|---|---|---|
| 17 | 0.017 | 237 | 0.0105 |
| 18 | 0.0163 | 238 | 0.0106 |
| 24 | 0.016 | 262 | 0.0105 |
| 24 | 0.0161 | 262 | 0.0103 |
| 55 | 0.0165 | 292 | 0.0099 |
| 58 | 0.0155 | 298 | 0.0101 |
| 82 | 0.0147 | 322 | 0.0098 |
| 86 | 0.0146 | 332 | 0.0100 |
| 101 | 0.0138 | 342 | 0.0097 |
| 106 | 0.0137 | 364 | 0.0094 |
| 132 | 0.0133 | 379 | 0.0094 |
| 135 | 0.0131 | 394 | 0.0095 |
| 159 | 0.0124 | 409 | 0.0093 |
| 161 | 0.0122 | 430 | 0.0086 |
| 188 | 0.0117 | 442 | 0.0089 |
| 191 | 0.0115 | 448 | 0.0089 |
| | | 460 | 0.0088 |
| 202 | 0.0109 | 476 | 0.0087 |
| 211 | 0.0112 | 493 | 0.0086 |
| 211 | 0.0113 | 501 | 0.0082 |
| 212 | 0.0113 | | |

the inert gas, $P_\ell$ and $P_g$. The analytical relation among these parameters is,

$$P = \frac{2\delta}{r} + h(P_\ell - P_g). \qquad (9)$$

At a fixed immersion depth, the pressure of the gas is an inverse function of the radius of curvature of the bubble. The maximum pressure occurs at the minimum radius of curvature of the bubble which is fixed by the geometry of the capillary tube. The procedure for determining the density of the liquid consists of measuring the maximum pressure of the inert gas during the formation and release of the bubble from the end of the capillary tube at a fixed immersion depth. The capillary tube is repositioned at a different depth and the maximum bubble pressure is measured at this new depth. These experimental data, the maximum bubble pressure versus the immersion depth, are fitted to a linear equation by the method of least squares. The slope of the fitted curve is the value for the difference between the densities of the liquid phase and the inert gas. In all of the experiments argon was used as the inert gas. Since the value of the density of the liquid phase is more than 1000 times that of the gas, the value of the slope of the fitted curve was taken as the density of the liquid.

### 3.4.1 Apparatus and Calibration Tests

The main features of the apparatus which was used for the measurement of the liquid density are illustrated in Figure 3. The capillary tube was mounted on a carriage whose vertical position was controlled by the threaded rod. The D.C. electric motor was energized to turn the threaded rod which changed the position of the capillary tube. The vertical position of the carriage for the capillary tube was determined by the output signal of the potentiometer. The potentiometer was fixed onto the base of the apparatus and the rotor of the potentiometer was connected by a flexible wire to the capillary carriage. The specimen was held in the furnace cavity by a

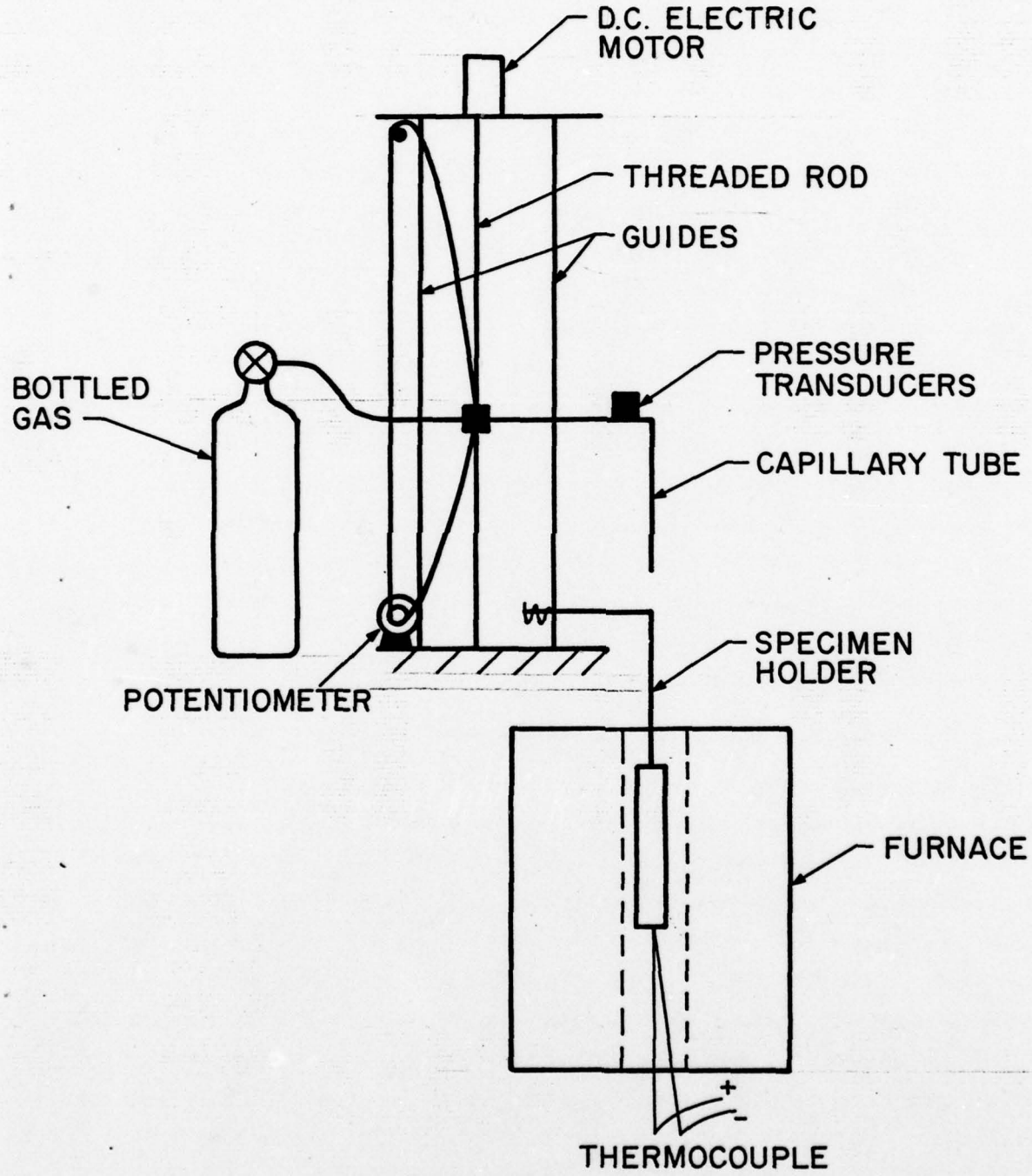


Figure 3. Maximum Bubble Pressure Apparatus for Measurement of Liquid Densities at Elevated Temperatures.

fixture which was rigidly fixed to the base of the apparatus. The guides insured that the capillary tube and the specimen were properly aligned. The temperature of the specimen was sensed by a chromel-alumel thermocouple which was placed in contact with the specimen holder. The pressure of the gas and its flow rate were sensed by pressure transducers located in the gas line.

The entire apparatus was calibrated with distilled water at room temperature. The distilled water sample was inserted into the specimen holder and the capillary tube was immersed into the water. The pressure of the gas was measured during the bubbling process at two different flow rates. The reported value for the density of water* and the data for the maximum pressure versus the immersion depth were combined with the first derivative of equation 9 in the form,

$$K = \frac{1}{P_{H_2O}} \frac{\partial}{\partial h} P_{max} \qquad (10)$$

to determine the apparatus constant, K. The immersion depth was sensed by a Spectral potentiometer, model number SC-1, whose output signal was displayed on a Fluke voltmeter, model number 8300A. The pressure and flow rate of the gas were detected by Weston pressure transducers, model number 731. The output of these pressure transducers was displayed on a Honeywell X-Y recorder, model number 560. The temperature of the water was sensed by the chromel-alumel thermocouple whose output was displayed on an Omega digital thermometer, model number 2809. The data collected for the calibration experiments are presented in Table 8.

The accuracy of this technique was assessed** by measuring of densities of toluene and of methylene chloride.

---

*Handbook of Chemistry and Physics, The Chemical Rubber Company, Cleveland, Ohio, 1968.

The measured values differed from tabulated values by less than 0.5 percent.

### 3.4.2 High Temperature Liquid Density Measurements

The measurement of the density of the eutectic liquid was performed at a temperature of 775°C. The eutectic liquid specimens were contained in an Inconel 617 alloy crucible for these measurements. The procedure described in Section 3.4 was employed for the measurements. The separate determinations were made of the liquid density. Each of the ten determinations consisted of at least eight measurements of the maximum bubble pressure at a fixed immersion depth of the capillary tube. The values of the liquid density for each determination are presented in Table 9. The average value of the liquid density was determined to be 2.009 grams per cubic centimeter at 775°C.

The value for the density of the solid eutectic composition was measured at 22.8°C by comparing the weight of the specimen in air with the weight of the specimen submerged in water. The average value of the solid density for measurements on two specimens was determined to be 2.305 $\pm$ 0.005 grams per cubic centimeter.

The value change of the eutectic between the solid at 22.8°C and the liquid phase at 775°C was calculated to be 14.7 percent.

## 4.0 CONCLUSIONS

The liquid-solid transformations of inorganic oxide-fluoride compositions were assessed to determine their potential for thermal energy storage applications. The data available for the enthalpy of fusion of the pure components was sufficient to

---

**AFAPL-TR-77-70, "Feasibility Study of Inorganic Oxides for Thermal Energy Storage Applications," Air Force Aero Propulsion Laboratory, Wright-Patterson Air Force Base, Ohio 45433.

TABLE 8

DETERMINATION OF THE APPARATUS CONSTANT, K,
FOR THE LIQUID DENSITY MEASUREMENTS

Probe: Stainless Steel
Temperature: 24°C
Gas: Argon

| Cycle | K (milliliters/gram/millivolts/volt) |
|---|---|
| 1 | -1.257 |
| 2 | -1.255 |
| 3 | -1.250 |
| 4 | -1.250 |
| 5 | -1.257 |
| 6 | -1.253 |
| 7 | -1.249 |
| 8 | -1.252 |
| avg. | -1.253 ± 0.003 |

TABLE 9

THE LIQUID DENSITY OF THE LiF-$Li_2O$-$B_2O_3$
EUTECTIC AT 775°C (Argon Gas)

| Cycle | Density grams/cc |
|---|---|
| 1 | 2.017 |
| 2 | 1.996 |
| 3 | 1.996 |
| 4 | 1.999 |
| 5 | 2.033 |
| 6 | 2.038 |
| 7 | 2.015 |
| 8 | 2.021 |
| 9 | 1.981 |
| 10 | 1.996 |
| avg. | 2.009 ± 0.018 |

determine those pure oxides and fluorides which have a high potential. However, the temperature-composition phase diagrams of the oxide-fluoride systems which have been compiled are not sufficient to permit an exhaustive assessment of the liquid-solid transformation in many oxide-fluoride systems of interest. There are no oxide-fluoride phase diagrams available which contain one of the oxides, $ThO_2$, BeO, VO, or TiO. All of the pure oxides have a value for the enthalpy of fusion which is greater than 794 Joules per gram (100 watt-hours per pound). Indeed the oxide, $ThO_2$, has a value for the enthalpy of fusion which is 4610 Joules per gram. Of the seventy oxide-fluoride systems which were reviewed, five contain liquid-solid transformation in the temperature range 537 to 560°C (1000-1400°F). The eutectic composition at twenty weight percent lithium fluoride of the $LiF-Li_2O-B_2O_3$ system was selected for experimental characterization on the basis of the reported value for the eutectic temperature and the estimated value for the enthalpy of transformation. The value which was measured for the enthalpy of transformation of this eutectic composition is 672 Joules per gram which compares to a value of 754 Joules per gram for the ternary eutectic fluoride composition of the $LiF-MgF_2-KF$ system. The values for the thermal diffusivity which have been measured from room temperature up to 500°C for the oxide-fluoride eutectic are approximately the same as those measured on the ternary eutectic fluoride. Because of the larger value associated with the enthalpy of transformation of the eutectic composition of the $LiF-MgF_2-KF$ system as compared to that of the $LiF-Li_2O-B_2O_3$ system, the ternary fluoride is recommended for thermal energy storage applications.

# APPENDIX A

## REVIEW OF LIQUID-SOLID PHASE EQUILIBRIUM IN SELECTED INORGANIC OXIDE-FLUORIDE SYSTEMS

$LiF-B_2O_3$

The only reported intermediate phase, $LiF \cdot B_2O_3$, melts at 840°C. There is an eutectic transformation reported between the phases, LiF and $LiF \cdot B_2O_3$, at a composition of 50 mole percent LiF and at a temperature of 798°C. A horizontal liquidus is depicted at 835°C over a composition range of 65 to 90 mole percent $Li_2F_2$.

$LiF-AlF_3-Al_2O_3$

An eutectic transformation is depicted between $Li_3AlF_6$ and $Al_2O_3$ at a temperature of 775°C and 99 mole percent $Li_3AlF_6$.

$LiF-B_2O_3-BaF_2$

A ternary eutectic exists at a temperature of 745°C and a composition of 48 mole percent $Li_2F_2$ and 23 mole percent $B_2O_3$.

$LiF-B_2O_3-Li_2O$

The compound $LiBO_2$ melts at a temperature of 843°C. The compound $2LiF \cdot 3LiBO_2$ melts at a temperature of 755°C. The eutectic reaction between $LiBO_2$ and $2LiF \cdot 3LiBO_2$ occurs at 710°C and at a composition of 20 percent LiF. The eutectic reaction between LiF and $2LiF \cdot 3LiBO_2$ occurs at 688 at 35 percent LiF.

$LiF-GeO_2-MgO$

INSUFFICIENT DATA. (Only compatibility relations at 1000°C are reported, liquidus conditions had not been studied.)

$LiF-K_2O-TiO_2$

The reported phase diagram is probably in error. The eutectic composition at 680°C and 15 mole percent LiF most probably involves LiF and $Li_2TiO_3$. (See the $NaF-Li_2O-TiO_2$, the $KF-Li_2O-TiO_2$, and the $Li_2ORbF-TiO_2$ systems.)

$LiF-Li_2O-MoO_3$

The compound, $Li_2MoO_4$, melts without change in composition at 700°C. An eutectic exists at 62 mole percent $Li_2MoO_4$ at a temperature of 620°C between the LiF and $Li_2MoO_4$ solid phases.

$LiF-Li_2O-V_2O_5$

The compound $LiVO_3$ melts congruently at a temperature of 621°C. An eutectic between the $LiVO_3$ and LiF solid phases exists at a temperature of 583°C and at a composition of 75 mole percent $LiVO_3$.

$LiF-Li_2O-WO_3$

The compound, $Li_2WO_4$, melts congruently at a temperature of 740°C and an eutectic exists between the $Li_2WO_4$ and the LiF solid phases at a temperature of 640°C and at a composition of 62 mole percent $Li_2WO_4$.

$MgF_2-MgO$

An eutectic has been reported at a temperature of 1214°C between $MgF_2$ and MgO at a composition of 90 mole percent $MgF_2$.

$MgF_2-GeO-MgO$

Liquidus transformation had not been studied. Only the solid phase compatibility relations among the components have been reported.

$MgF_2-KF-SiO_2$

The liquidus data presented in the phase diagram are insufficient to determine the temperature and composition of liquid-solid transformations.

$MgF_2-MgO-SiO_2$

All of the liquid-solid transformations depicted in the phase diagram are greater than 1190°C.

$MgO-NaF-SiO_2$

The liquidus data presented in the phase diagram are insufficient to determine the compositions and temperatures of liquid-solid transformations.

$NaF-Al_2O_3$

The phase diagram between these two components shows an eutectic reaction at 985°C and 6 percent $Al_2O_3$. The data presented indicate that this system is a pseudobinary data and consequently the system is not suitable for the intended application.

$NaF-AlF_3-Al_2O_3$

The compound, $Na_3AlF_3$, melts congruently at a temperature of 1005°C. An eutectic transformation has been reported at a temperature of 962°C and 11 percent $Al_2O_3$ between $Na_3AlF_6$ and $Al_2O_3$.

$NaF-AlF_3-CaO$

An eutectic reaction exists between $Na_3AlF_6$ and CaO at a temperature of 896°C and 11 percent CaO.

$NaF-AlF_3-CdO$

An eutectic reaction between $Na_3AlF_6$ and CdO exists at a temperature of 970°C and 6 percent $CdO \cdot NaF-AlF_3-CeO_2$. The phase diagram suggests an extended solid solution phase of $CeO_2$ in $Na_3AlF_6$ with a minimum in the liquidus boundary at a temperature of 880°C and at a composition of 5 mole percent $CeO_2$.

$NaF-AlF_3-MgO$

The eutectic reaction between $Na_3AlF_6$ and MgO is reported at 900°C and at 7 percent MgO.

$NaF-AlF_3-Nd_2O_3$

The data presented in the phase diagram is insufficient to determine the temperature and composition of the liquid-solid transformation.

$NaF-AlF_3-Sm_2O_3$

The shape of the liquidus suggests that the liquid-solid transformation is probably characterized by a monotectic reaction at a temperature of 900°C and at a composition range of 2 to 6 mole percent $Sm_2O_3$.

$NaF-AlF_3-TiO_2$

The eutectic transformation is reported between $Na_3AlF_6$ and $TiO_2$ at a temperature of 970°C and 4 percent $TiO_2$.

$NaF-AlF_3-ZnO$

The eutectic transformation is reported between $Na_3AlF_6$ and $TiO_2$ at a temperature of 973°C and at a composition of 2.5 percent ZnO.

$NaF-AlF_3-ZrO_2$

The eutectic transformation between $Na_3AlF_6$ and $ZrO_2$ is reported at a temperature of 968°C and at a composition of 14 percent $ZrO_2$.

$NaF-B_2O_3-Na_2O$

The compound, $Na_2B_4O_7$, melts congruently at a temperature of 742°C. An eutectic reaction between $Na_2B_4O_7$ and NaF occurs at a temperature of 680°C and at a composition of 20 mole percent $Na_2F_2$.

$NaF-BaF_2-TiO_2$

The data is insufficient on this system to determine the temperature and composition of the liquid-solid transformation.

$NaF-BaO-TiO_2$

An eutectic reaction occurs between $Na_2F_2$ and $BaTiO_3$ at a temperature of 952°C and at a composition of 93 mole percent $Na_2F_2$.

$NaF-CaF_2-SiO_2$

The data is insufficient to determine the temperature and composition of the liquid-solid transformations.

$NaF-Na_2O-CrO_3$

The compound, $Na_2CrO_4$, melts at a temperature of 798°C. The eutectic reaction between $Na_2CrO_4$ and NaF occurs at a temperature of 650°C and at a composition of 38 mole percent NaF.

$NaF-Li_2O-TiO_2$

The phase diagram shows an eutectic reaction at 874°C and at a composition of 25 mole percent $Li_2TiO_3$. An independent investigation places the eutectic temperature at 844°C.

$NaF-MgF_2-SiO_2$

The data on this system is insufficient to locate the temperature or composition of the liquid-solid transformations.

$NaF-Na_2O-MoO_3$

The compound $Na_2MoO_4$ melts at a temperature of 690°C. The eutectic reaction between $Na_2MoO_4$ and NaF occurs at a temperature of 625°C and at a composition of 15 mole percent NaF.

$NaF-Na_2O-P_2O_5$

The compound, $NaPO_3$, melts at a temperature of 622°C. The compound, $NaF \cdot NaPO_3$, melts at a temperature of 635°C. An eutectic reaction between $NaPO_3$ and $NaF \cdot NaPO_3$ occurs at a temperature of 490°C and at a composition of 28 mole percent NaF. The eutectic reaction between $NaF \cdot NaPO_3$ and NaF occurs at a temperature of 614°C and at a composition of 55 mole percent NaF.

$NaF-Na_2O-SiO_2$

The compound, $Na_2SiO_3$, melts at a temperature of 875°C. The eutectic reaction between $Na_2SiO_3$ and NaF occurs at a temperature of 795°C and at a composition of 40 mole percent NaF.

$NaF-Na_2O-TiO_2$

The compound, $Na_2TiO_3$, melts at a temperature of 1020°C. An eutectic reaction is reported at a temperature of 898°C and at a composition of 30 mole percent NaF.

$NaF-Na_2O-V_2O_5$

The compound, $NaVO_3$, melts at a temperature of 636°C. The eutectic reaction between $NaVO_3$ and NaF occurs at a temperature of 599°C and at a composition of 15 mole percent NaF.

$NaF-Na_2O-WO_3$

The compound, $Na_2WO_4$, melts at a temperature of 690°C. The eutectic reaction between $Na_2WO_4$ and NaF occurs at a temperature of 640°C and at a composition of 20 mole percent NaF.

$NaF-PbO-TiO_2$

An eutectic reaction is reported between $Na_2F_2$ and $PbTiO_3$ at a temperature of 980°C and a composition of 2 mole percent $PbTiO_3$.

$NaF-SrF_2-SiO_2$

The data are insufficient to make a determination of the temperature or composition of the liquid-solid transformations.

$Li_2O-B_2O_3-LiF$ (see $LiF-B_2O_3-Li_2O$)

$Li_2O-KF-TiO_2$

The eutectic reaction occurs at 654°C and at a composition of 25 mole percent $Li_2TiO_3$.

$Li_2O$-LiF-$MoO_3$ (see LiF-$Li_2O$-$MoO_3$)

$Li_2O$-LiF-$V_2O_5$ (see LiF-$Li_2O$-$V_2O_5$)

$Li_2O$-LiF-$WO_3$ (see LiF-$Li_2O$-$WO_3$)

$Li_2O$-NaF-$TiO_2$ (see NaF-$Li_2O$-$TiO_2$)

$Li_2O$-RbF-$TiO_2$

The eutectic reaction occurs at a temperature of 651°C at a composition of 26 mole percent $Li_2TiO_3$.

MgO-$CaF_2$

The eutectic reaction occurs at a temperature of 1350°C and at a composition of 80 mole percent $CaF_2$.

MgO-$MgF_2$ (see $MgF_2$-MgO)

MgO-$AlF_3$-NaF (see NaF-$AlF_3$-MgO)

MgO-$CaF_2$-CaO

A ternary eutectic reaction occurs at a temperature of 1343°C at 10 weight percent MgO and 72 weight percent $CaF_2$.

MgO-$CaF_2$-$SiO_2$

The data are not sufficient to accurately locate the temperature and composition of the liquid-solid transformations for this system.

MgO-$GeO_2$-LiF (see LiF-$GeO_2$-MgO)

MgO-$GeO_2$-$MgF_2$ (see $MgF_2$-$GeO_2$-MgO)

MgO-$MgF_2$-$SiO_2$ (see $MgF_2$-MgO-$SiO_2$)

$Al_2O_3$-CaF

The eutectic reaction occurs at a temperature of 1260°C at a composition of 28 percent $Al_2O_3$.

$Al_2O_3$-NaF (see NaF-$Al_2O_3$)

$Al_2O_3$-$AlF_3$-LiF (see LiF-$AlF_3$-$Al_2O_3$)

$Al_2O_3$-$AlF_3$-NaF (see NaF-$AlF_3$-$Al_2O_3$)

$Al_2O_3$-$CaF_2$-CaO

The ternary eutectic reaction is at 1310°C at a composition of 20 percent $5CaO \cdot 3Al_2O_3$ and 65 percent $CaF_2$.

$Al_2O_3$-$CaF_2$-$SiO_2$

All liquid-solid transformations occur above 1220°C.

$Al_2O_3$-$CaF_2$-$TiO_2$

All liquid-solid transformations occur above 1280°C.

CaO-$CaF_2$

An eutectic reaction is postulated at a temperature of 1360°C and at a composition of 83 mold percent $CaF_2$.

CaO-$AlF_3$-NaF (see NaF-$AlF_3$-CaO)

CaO-$Al_2O_3$-$CaF_2$ (see $Al_2O_3$-$CaF_2$-CaO)

CaO-$CaF_2$-FeO

The data on this system are not sufficient to accurately locate the temperature and composition of liquid-solid transformations.

CaO-$CaF_2$-MgO (see MgO-CaO-$CaF_2$)

CaO-$CaF_2$-$P_2O_5$

The compound, $CaF_2 \cdot 3Ca_3(PO_4)_2$, melts at a temperature of 1650°C. The eutectic reaction between this compound and $CaF_2$ occurs at 1205°C at 60 mole percent $CaF_2$.

$CaO-CaF_2-SiO_2$

A ternary eutectic reaction is located at 1113°C at a composition of 16 percent $SiO_2$ and 40 percent CaO. A second ternary eutectic reaction occurs at 1115°C at a composition of 12 percent $SiO_2$ and 53 percent CaO.

$TiO_2-CaF$

The eutectic reaction occurs at a temperature of 1360°C at a composition of 57 weight percent $TiO_2$.

$TiO_2-AlF_3-NaF$ (see $NaF-AlF_3-TiO_2$)

$TiO_2-AlF_3-CaF$

All of the liquid-solid transformations occur at a temperature greater than 1280°C.

$TiO_2-BaO-KF$

The eutectic reaction between KF and $BaTiO_3$ occurs at a temperature of 830°C and at 97.5 mole percent KF.

$TiO_2-BaO-NaF$ (see $NaF-BaO-TiO_2$)

$TiO_2-KF-LiO_2$

The eutectic reaction occurs at a temperature of 654°C and at a composition of 25 mole percent $Li_2TiO_3$.

$TiO_2-KF-PbO$

The eutectic reaction between $PbTiO_3$ and $K_2F_2$ occurs at 845°C and 15 mole percent $PbTiO_3$.

$TiO_2-K_2O-LiF$ (see $LiF-K_2O-TiO_2$)

$TiO_2-Li_2O-RbF$ (see $Li_2O-RbF-TiO_2$)

$TiO_2-NaF-Na_2O$ (see $NaF-Na_2O-TiO_2$)

$TiO_2-NaF-PbO$ (see $NaF-PbO-TiO_2$)

# APPENDIX B

## THE APPLICATION OF THE PHASE DIAGRAM TO THERMAL ENERGY STORAGE TECHNOLOGY

(The work contained in this Appendix was presented at The Workshop on Phase Diagrams in Metallurgy and Ceramics at the National Bureau of Standards, Gaithersburg, Maryland, January 10-12, 1977.)

National Bureau of Standards SP-496, Applications of Phase Diagrams in Metallurgy and Ceramics
Proceedings of Workshop held at NBS, Gaithersburg, Md., January 10-12, 1977

# THE APPLICATION OF THE PHASE DIAGRAM TO THERMAL ENERGY STORAGE TECHNOLOGY

Jerry E. Beam
Air Force Aero Propulsion Laboratory
Wright-Patterson Air Force Base, OH 45433

and

Joseph E. Davison, Ph.D.
University of Dayton Research Institute
Dayton, OH 45469

## 1.0 INTRODUCTION

In our program, we are evaluating the potential of phase change thermal energy storage devices to provide heat energy to operate a Vuillieumier cooler for space satellite applications. We have selected the liquid-solid transformation as the energy storage mechanism. Our next step has been to identify liquid-solid transformations which have the largest storage capacity in the temperature range for our application. In this presentation, we have identified those pure components which are of primary interest and the type of data available in the phase diagram which can be utilized to assess the relative merits of different materials.

## 2.0 SELECTION OF MATERIALS

The tabulated values for the enthalpy of fusion and the melting temperature of the pure components provide a quantitative basis for the selection of phase change thermal energy storage materials. Values for selected elements, inorganic oxides, and inorganic fluorides are presented in Table 1. Extensive compilations of these values for different classes of pure components have been prepared and are available (1-11). The selection of a pure component as the energy storage media limits the application temperature to the melting temperature of the component. This limitation can be circumvented to some extent by selecting intermediate compositions between or among pure components. These intermediate compositions can be readily identified from the appropriate phase diagram. As an example, the melting points of the fluorides of lithium and magnesium are respectively 848°C and 1242°C.

TABLE 1

SELECTED VALUES FOR THE ENTHALPY OF FUSION AND THE MELTING TEMPERATURE

| | Enthalpy of Fusion | Melting Temperature | |
|---|---|---|---|
| | K Joules/gram | Deg. C | Ref. |
| a. Elements | | | |
| Carbon | (8.71) | (4327) | 5 |
| Boron | (2.05) | 2027 | 5 |
| Silicon | 1.80 | 1412 | 5 |
| Beryllium | 1.36 | 1287 | 5 |
| Phosphorus (red) | 0.61 | 597 | 1 |
| Germanium | 0.51 | 937 | 5 |
| Lithium | 0.43 | 181 | 5 |
| Vanadium | (0.41) | 1902 | 5 |
| Aluminum | 0.40 | 660 | 5 |
| b. Oxides | | | |
| $ThO_2$ | 4.61 | 2952 | 3 |
| BeO | 2.53 | 2547 | 1 |
| $Li_2O$ | (1.96) | 1570 | 1 |
| MgO | (1.92) | 2825 | 1 |
| $Al_2O_3$ | 1.16 | 2042 | 1 |
| c. Fluorides | | | |
| LiF | 1.04 | 848 | 1 |
| $MgF_2$ | 0.93 | 1242 | 1 |
| NaF | 0.79 | 996 | 1 |
| $CaF_2$ | 0.61 | 1127 | 1 |
| $FeF_2$ | (0.55) | (1100) | 1 |
| $ScF_3$ | 0.49 | 1227 | 3 |
| $TiF_3$ | 0.48 | 1227 | 3 |
| KF | 0.47 | 858 | 1 |

The phase relations in the binary system of these two components has been studied (11,12) and an eutectic transformation has been identified at 724°C and at 33 mode percent $MgF_2$. Additional invariant points of ternary eutectic compositions at lower temperatures may be obtained by adding NaF or KF. Thus, the temperature of the liquid-solid transformation can be tailored to the particular application. The types of liquid-solid transformations which

we have identified for our applications are the eutectic transformation and the congruent melting of an intermediate compound. The selection of these transformations is based on their reproducibility during cycling between the liquid and solid states. Although the peritectic reaction is reversible in a thermodynamic sense, the time required to attain an equilibrium state on cooling through the peritectic horizational was judged to be unsatisfactory for short duty cycles.

## 2.1 THE ENTHALPY OF THE LIQUID-SOLID TRANSFORMATION

The amount of heat energy which can be stored or released in the isothermal and reversible transformation between a pure solid and liquid phase at constant pressure is obtained directly from the value for the enthalpy of fusion of the substance. However, when two solid phases of different compositions react to form a single liquid phase, then the value for the enthalpy of mixing must be taken into account to determine the amount of heat energy involved in the liquid-solid transformation.

The effect of the enthalpy of mixing on the energy storage capacity of a liquid-solid transformation can be assessed by consideration of the following thermodynamic cycle. The isothermal and reversible reaction between two solid phases may be considered as the sum of the following processes:

$$\begin{array}{ccccc} n\,A(\ell) & + & m\,B(\ell) & \xrightarrow{\text{step 3}} & (n+m)\;\; AB(\ell, \text{sol'n}), \quad T_2 \\ \text{step 1}\uparrow & & \text{step 2}\uparrow & & \text{step 4}\downarrow \\ n\,A(s) & + & m\,B(s) & \xrightarrow{\text{step 5}} & (n+m)\;\; AB(\ell, \text{sol'n}), \quad T_1 \end{array} \qquad (1)$$

Step 1: Heat "n" moles of component A from temperature $T_1$ to $T_2$. The enthalpy change of this step is given by,

$$\Delta H_1 = n \int_{T_1}^{T_A} C_{P,A}\,dT + n\,\Delta H_{M,A} + n \int_{T_A}^{T_2} C_{P,A}\,dT, \qquad (2)$$

where $T_A$ represents the melting point of pure A.

Step 2: Heat "m" moles of component B from temperature $T_1$ to $T_2$. The enthalpy change for this step is given by,

$$\Delta H_2 = m \int_{T_1}^{T_B} C_{P,B} dT + m \Delta H_{M,B} + m \int_{T_B}^{T_2} C_{P,B} dT, \quad (3)$$

where $T_B$ represents the melting point of pure B.

Step 3: React the two separate liquid components to form the AB liquid solution at a temperature of $T_2$. The enthalpy change for this step is given by,

$$\Delta H_3 = (n+m) \ \Delta H \text{ (mix)}. \quad (4)$$

Step 4: Cool the AB liquid solution from temperature $T_2$ to $T_1$. The enthalpy change for this step is given by,

$$\Delta H_4 = (n+m) \int_{T_2}^{T_1} C_{P,AB} dT. \quad (5)$$

Step 5: The value for the enthalpy of the liquid-solid transformation between the two solid phases, A and B, and the liquid solution, AB, at the temperature, $T_1$, can be expressed as the sum of the enthalpies of the first four steps, and is as follows,

$$\Delta H_5 = n \Delta H_{M,A} + m \Delta H_{M,B} + (n+m) \Delta H(\text{mix.}) +$$

$$n \int_{T_1}^{T_A} C_{P,A} dT + n \int_{T_A}^{T_2} C_{P,A} dT + m \int_{T_1}^{T_B} C_{P,B} dT +$$

$$m \int_{T_B}^{T_2} C_{P,B} dT + (n+m) \int_{T_2}^{T_1} C_{P,AB} dT. \quad (6)$$

In the absence of data for the heat capacities of the liquid phase, the Neumann-Kopf Rule states that the heat capacity of a substance may be taken as the sum of the heat capacities of the elemental constituents. The application of this rule in the present analysis gives a zero value to the sum of heat capacity terms. As a result, the heat energy which can be stored in the isothermal liquid-solid transformation is given by,

$$\Delta H_5 \approx n\,\Delta H_{M,A} + m\,\Delta H_{M,B} + (n+m)\,\Delta H(\text{mix}). \qquad (7)$$

The first two terms on the right-hand side of this expression are properties of the individual components. The last term on the right is the contribution due to the enthalpy of mixing. The effect of the enthalpy of mixing on the heat of the liquid-solid transformation can be either positive or negative depending on whether the reaction is endothermic or exothermic. If the reaction is endothermic, then the enthalpy of mixing is positive and additional heat energy can be stored in the transformation. If the reaction is exothermic, then the converse is true and less heat energy can be stored in the transformation than would be predicted from the properties of the individual components.

Unfortunately, the data for the enthalpy of mixing are available for relatively few systems. In order to obtain values for the enthalpy of mixing we have combined experimental data which is presented in the phase diagrams with analytical thermodynamic models to obtain the required data.

## 2.2 THE ENTHALPY OF MIXING

Analytical expressions for the liquidus and solidus phase boundaries can be obtained by combining basic thermodynamic principles with a thermodynamic model of the alloying behavior of the system. When the regular solution model is utilized to represent the alloying characteristics of the system, the following expressions have been obtained for the liquidus and solidus boundaries (13).

$$\Delta H_{fA}(T/T_A - 1) - RT \ln (X_A^{\alpha}/X_A^{L}) = W_1^{\alpha}(X_B^{\alpha})^2 - W_1^{L}(X_B^{L})^2, \qquad (8)$$

and

$$\Delta H_{fB}(T/T_B - 1) - RT \ln (X_B^{\alpha}/X_B^{L}) = W_1^{\alpha}(X_A^{\alpha})^2 - W_1^{L}(X_A^{L})^2. \qquad (9)$$

The values of the parameters, $W^{\alpha}$ and $W_1^L$, were calculated from Equations (8) and (9) with the known values for the enthalpies of fusion, $\Delta H_{fA}$ and $\Delta H_{fB}$, the melting points, $T_A$ and $T_B$, of the pure constituents, and the composition of the liquidus boundary, $X_A^L$ and $X_B^L$, and the solidus boundaries, $X_A^{\alpha}$ and $X_B^{\alpha}$, at the temperature, T. The enthalpy of mixing of the liquid solution is related to the parameter, $W_1^L$, by the expression,

$$\Delta H \text{ (mix)} = X_A^L X_B^L W_1^L. \qquad (10)$$

An underlying assumption in this approach is that the crystal structures of the two solid phases, A and B, are the same. If the crystal structures are different, then the enthalpy of the solid state transformation between the two structures must be known to obtain an exact solution. In the absence of any data, a zero value was assigned to the enthalpy of the solid state transformation. The data taken from selected phase diagrams and the results of the computations for the parameters $W_L$ and $W_S$ are presented in Table 2. The values of the composition of the solidus boundary were available on only a few of the systems studied. In the absence of any experimental data, a value of 0.999999 was assigned to the solidus composition. The calculated values for the enthalpy of mixing at a mole fraction of 0.5 are compared to experimental values which have been measured on these systems in Table 3. The negative values for the enthalpy of mixing have the effect of decreasing the energy storage capacity of the binary systems in accord with the relation 7. However, the magnitude of the decrease for the system, LiF - KF, represents less than 15 percent of the value for the enthalpy of fusion of the LiF.

## 3.0 SPECIFIC USER NEEDS

The phase diagrams which are of special interest to a phase change thermal storage technology base for space satellite applications are those which have the largest value for the enthalpy of the liquid-solid transformation

TABLE 2

EXPERIMENTAL DATA FOR THE TEMPERATURE AND COMPOSITION OF THE LIQUIDUS AND SOLIDUS PHASE BOUNDARIES

| System A | System B | Temp. Deg. C | Mole Fraction Liquidus | Mole Fraction Solidus | $W_L$ K Joules per Mole | $W_S$ K Joules per Mole |
|---|---|---|---|---|---|---|
| a. Chlorides: | | | | | | |
| AgCl | KCl | 306 | 0.695 | * | -10.2 | --- |
| $AlCl_3$ | KCl | 250 | 0.495 | * | -40.5 | --- |
| $AlCl_3$ | NaCl | 152 | 0.490 | * | -60.4 | --- |
| $CaCl_2$ | $FeCl_2$ | 592 | 0.445 | * | 4.0 | --- |
| $CaCl_2$ | $MgCl_2$ | 621 | 0.428 | 0.877 | 5.3 | 20.1 |
| $CaCl_2$ | NaCl | 500 | 0.52 | * | -11.4 | --- |
| $FeCl_2$ | NaCl | 370 | 0.43 | * | -19.4 | -4.8 |
| $FeCl_3$ | NaCl | 158 | 0.54 | * | -39.5 | --- |
| KCl | LiCl | 358 | 0.586 | * | -16.8 | --- |
| LiCl | RbCl | 312 | 0.5525 | * | -19.2 | --- |
| b. Fluorides: | | | | | | |
| KF | LiF | 492 | 0.5 | * | -17.2 | --- |
| KF | $MgF_2$ | 778 | 0.85 | * | -47.6 | --- |
| KF | NaF | 710 | 0.6 | 0.88 | -0.01 | 22.4 |
| LiF | $MgF_2$ | 724 | 0.68 | 0.94 | -1.3 | 37.5 |
| LiF | NaF | 649 | 0.61 | * | -6.4 | --- |
| LiF | RbF | 450 | 0.47 | * | -18.0 | --- |
| $MgF_2$ | NaF | 987 | 0.64 | * | -39.5 | --- |
| $MgF_2$ | RbF | 883 | 0.625 | * | -65.9 | --- |
| NaF | RbF | 664 | 0.33 | * | -0.1 | --- |
| c. Oxides: | | | | | | |
| $B_2O_3$ | $Li_2O$ | 715 | 0.55 | * | -27.2 | --- |
| $Bi_2O_3$ | $Li_2O$ | 730 | 0.92 | * | -272. | --- |
| $Li_2O$ | $MoO_3$ | 570 | 0.75 | * | -25.3 | --- |
| $Li_2O$ | $V_2O_5$ | 621 | 0.835 | * | -10.4 | --- |
| $Li_2O$ | $WO_3$ | 800 | 0.63 | * | -41.1 | --- |

* In the absence of any experimental information, the mole fraction of the solidus boundary is assumed to be 1.000.

TABLE 3

CALCULATED AND EXPERIMENTAL VALUES
FOR THE ENTHALPY OF MIXING

| System | | $\Delta H$ mix, N = 0.5 K Joules per Mole Calc. | Exp. |
|---|---|---|---|
| AgCl | KCl | -2.5 | -0.84[1], -2.31[2] |
| KCl | LiCl | -4.2 | -4.39[2], -3.98[3] |
| LiCl | RbCl | -4.8 | -5.02[2] |
| LiF | KF | -4.3 | -4.47[3] |
| $Li_2O \cdot 2B_2O_3$* | | -6.0* | -3.3[4]* |

1. K. Stern, J. Phys. Chem. 60, 679, (1956).
2. L. S. Hersch, O. J. Kleppa, J. Phys. Chem. 42, 3752, (1956).
3. E. Aukrost, B. Bjorge, H. Flood, T. Forlan, Amer. N.Y. Acad. Sci. 79, 830, (1960).
4. JANAF Thermochemical Tables, Dow Chemical Company, Midland, Mich. (1962).

* The calculated and experimental values are for the composition of $Li_2O \cdot 2B_2O_3$.

on a per-unit mass basis. The value for this transformation depends for the most part on the values of the enthalpy of fusion of the pure components and the enthalpy of mixing of the pure components in the liquid phase. The pure components can be selected on the basis of the tabulated values for their enthalpies of fusion. In Table 1 we presented these values for metal oxides and metal fluorides which have the largest values in their respected groups on a per gram basis. Next, we reviewed the number of phase diagrams compiled by the American Ceramic Society (14) which contain one of these pure components. In Table 4 are tabulated the pure component and the total number of phase diagrams presented which contain that component, and many of the systems which have been compiled have been only partially investigated. More comprehensive coverage of systems which contain these components would be of significant value in the selection process.

TABLE 4

THE NUMBER OF PHASE DIAGRAMS COMPILED WHICH CONTAIN A PURE COMPONENT WITH A LARGE VALUE FOR THE ENTHALPY OF FUSION ON A PER-UNIT WEIGHT BASIS

| System | Total No. of Systems | No. of Binary Systems | No. of Ternary Systems |
|---|---|---|---|
| LiF | 128 | 42 | 50 |
| $MgF_2$ | 27 | 12 | 14 |
| NaF | 195 | 46 | 91 |
| $CoF_2$ | 3 | 3 | 0 |
| $FeF_2$ | 2 | 2 | 0 |
| $ScF_3$ | 8 | 6 | 2 |
| $TiF_3$ | --- | -- | -- |
| KF | 134 | 37 | 52 |
| $ThO_2$ | 25 | 13 | 11 |
| BeO | 36 | 17 | 18 |
| $Li_2O$ | 94 | 16 | 52 |
| MgO | 158 | 35 | 70 |
| $Al_2O_3$ | 207 | 53 | 70 |

The data of primary interest within a particular system are the composition, temperature, and type of liquid-solid transformation.

An assessment of the reliability and the accuracy of thermodynamic models to calculate the enthalpy of mixing from data presented in the phase diagram would likewise be of significant value. If this method can produce reliable thermodynamic data, then a significant increase in our data base for values for the enthalpy of mixing can be made available from the phase diagrams which have been compiled.

## 4.0 SUMMARY

The applications of the phase diagram to phase change energy storage technology has been presented. Our particular needs are for materials which have large values for the enthalpy of the liquid-solid transformations. Two properties which determine this enthalpy value are the enthalpies of fusion of the pure components and the enthalpy of mixing of the pure components. Values for the enthalpy of mixing can be determined from the data presented in the phase diagram when coupled with a thermodynamic model of the alloying behavior. We hope that our comments will have been of value to assist investigators in assessing the importance of phase diagrams in providing for a technology base for thermal energy storage.

## REFERENCES


1. JANAF Thermochemical Tables, 2nd Edition, Dow Chemical Company, Midland, Michigan.

2. Kabaschewski and Evans, Metallurgical Thermochemistry, 3rd Edition, Pergamon Press, New York, 1958.

3. Wicks and Block, Thermodynamic Properties of 65 Elements, Bureau of Mines Bulletin, 605, 1963.

4. Handbook of Materials Science, Volume 1, General Properties, CRC Press, Cleveland, Ohio, 1974.

5. Hultgren et al., Supplement to Selected Values of Thermodynamic Properties of Metals and Alloys, ASM, Metals Park, Ohio, 1974.

6. Thermal and Other Properties of Refractories, LA-5937-MS Informal Report dated March 1975 by Dwayne T. Vier of the Los Alamos Scientific Laboratory, Los Alamos, New Mexico.

7. Janz, George J., Molten Salts Handbook, Academic Press, New York, 1967.

8. Phase Change Materials Handbook, NASA Contractor Report Number NASA CR-61363, dated September 1971 by Hale, Hoover, and O'Neill of Lockheed Missiles and Space Company, Huntsville, Alabama.

9. Determination and Analysis of the Potentialities of Thermal Energy Storage Materials, ASD Technical Report 61-187 dated June 1961 by Wilson, Beahm, and Cooper of the Callery Chemical Company, Callery, Pennsylvania.

10. Survey and Selection of Inorganic Salts for Application to Thermal Energy Storage, ERDA-59 dated June 1975 by Alina Borucka, Borucka Research Company, Livingston, New Jersey.

11. Evaluation of Eutectic Fluoride Thermal Energy Storage Unit Compatibility, AFAPL-TR-79-92-Part 1 by Joseph E. Davison, dated October 1975, University of Dayton, Dayton, Ohio.

12. Voskresenskaya, N.K., Handbook of Solid-Liquid Equilibria in Systems of Anhydrous Inorganic Salts, Volume 1. Available from the U.S. Department of Commerce Clearinghouse for Federal Scientific and Technical Information, Springfield, Virginia.

## REFERENCES (concluded)


13. Davison and Rice, Application of Computer Generated Phase Diagrams to Composite Synthesis, NMAB 308-III, dated January 1973. Proceedings of the Conference on In-Situ Composites, September 5-8, 1972, Reported by the National Materials Advisory Board, Washington, D.C.

14. Levin, Robbins, and McMurdie, Phase Diagrams for Ceramists, 1964 (also see the 1969 and 1975 Supplements), The American Ceramic Society, Columbus, Ohio.